










Knockdown of GABA_A alpha3 subunits on thalamic reticular neurons enhances deep sleep in mice

David S. Uygun ¹, Chun Yang¹, Elena R. Tilli ², Fumi Katsuki ¹, Erik L. Hodges ¹, James T. McKenna ¹, James M. McNally ¹, Ritchie E. Brown ^{1,3} & Radhika Basheer ^{1,3} 

Identification of mechanisms which increase deep sleep could lead to novel treatments which promote the restorative effects of sleep. Here, we show that knockdown of the $\alpha 3$ GABA_A-receptor subunit from parvalbumin neurons in the thalamic reticular nucleus using CRISPR-Cas9 gene editing increased the thalamocortical delta (1.5–4 Hz) oscillations which are implicated in many health-promoting effects of sleep. Inhibitory synaptic currents in thalamic reticular parvalbumin neurons were strongly reduced *in vitro*. Further analysis revealed that delta power in long NREM bouts prior to NREM-REM transitions was preferentially affected by deletion of $\alpha 3$ subunits. Our results identify a role for GABA_A receptors on thalamic reticular nucleus neurons and suggest antagonism of $\alpha 3$ subunits as a strategy to enhance delta activity during sleep.

¹VA Boston Healthcare System and Harvard Medical School, Dept. of Psychiatry, West Roxbury, MA 02132, USA. ²Stonehill College, Department of Psychology, Easton, MA 02357, USA. ³These authors jointly supervised this work: Ritchie E. Brown, Radhika Basheer.
✉email: radhika_basheer@hms.harvard.edu

Sleep is vital for maintaining physical and mental well-being. In particular, thalamocortical delta (1.5–4 Hz) oscillations present in deep non-rapid-eye-movement (NREM) sleep are implicated in a wide range of processes beneficial to health including synaptic homeostasis, cellular energy regulation, clearance of toxic proteins, cognitive performance and mood^{1–4}. Conversely, insomnia, traumatic brain injury, obstructive sleep apnea, and other brain disorders are associated with interrupted/fragmented sleep, reduced deep NREM sleep and decreased delta wave power^{5–8}. Although hypnotic agents which potentiate the activity of GABA_A receptors promote sleep induction, they also reduce delta oscillations, suggesting that a subset of GABA_A receptors prevents deep restorative sleep^{9,10}. Thus, identification and elimination of this confounding effect of the most widely used hypnotics, which target GABA_A receptors, could be beneficial in developing drugs which boost the positive effects of sleep.

Delta oscillations during NREM sleep are primarily generated by thalamocortical relay neurons^{11–14}, which tend to discharge in bursts at delta frequencies when sufficiently hyperpolarized due to activation of a slow hyperpolarization-activated cation current and de-inactivation of low-threshold calcium channels^{15,16}. Hyperpolarization of thalamocortical relay neurons during NREM sleep is due to the withdrawal of excitatory neuromodulatory inputs and active inhibition mediated by the major GABAergic input from the thalamic reticular nucleus (TRN)^{11–13,15,16}. Recent work suggested that increased activity of TRN neurons plays a role in promoting delta power^{17–19} and NREM sleep^{20–23}. However, the role of the GABAergic receptors on TRN neurons in controlling sleep oscillations is not well understood.

Here we used state-of-the-art CRISPR-Cas9 gene editing to test the hypothesis that GABA_A receptors on TRN neurons suppress NREM sleep delta oscillations.

Results

Targeting the TRN for localized alpha3 (α3) KD. In the adult brain, most GABA_ARs consist of two α subunits (α1–6), two β subunits (β1–3), and one γ subunit (γ1–3)²⁴ (Fig. 1a). The α subunit is a necessary component of the GABA_AR, required for assembling a functional receptor²⁵. In the mouse thalamus, all synaptic GABA_ARs in thalamocortical relay nuclei contain the α1 subunit, whereas GABA_ARs in the TRN contain the α3 subunit²⁶. To introduce a brain region and cell-type-specific ablation of the α3 subunit gene, we first generated mice which expressed the Cas9 endonuclease in the major subset of TRN neurons which contain the calcium-binding protein parvalbumin (PV) by crossing PV-Cre mice with Rosa26-Lox-stop-lox-Cas9-GFP mice to produce PV-Cas9-GFP offspring. Next, we analyzed the gene sequence of the α3 subunit and selected three loci close to the start codon as target regions expected to maximize CRISPR-Cas9 mediated ablation (Fig. 1a). Our target regions were within the extracellular domain (Fig. 1a), the major ligand binding component, forming parts of the GABA binding site and the benzodiazepine binding site²⁷. We then constructed an adeno-associated viral (AAV) vector to target the α3 subunit (AAV5-α3-sgRNA-mCherry) by introducing the sequences for the single-guide RNAs (sgRNAs) into an AAV vector plasmid, each driven by the U6 promoter paired with mCherry as a red fluorescent marker (Fig. 1b). To test the effect of α3 knockdown (α3KD) on sleep and spectral activity, we recorded cortical oscillations using frontal electroencephalographic (EEG) electrodes and nuchal muscle electromyographic (EMG) electrodes before and after we introduced AAV-α3-sgRNA-mCherry into the TRN via chronically implanted guide cannulae (Fig. 1b).

NREM delta wave power is enhanced by α3KD in the TRN. α3KD in TRN PV neurons resulted in a marked increase in NREM

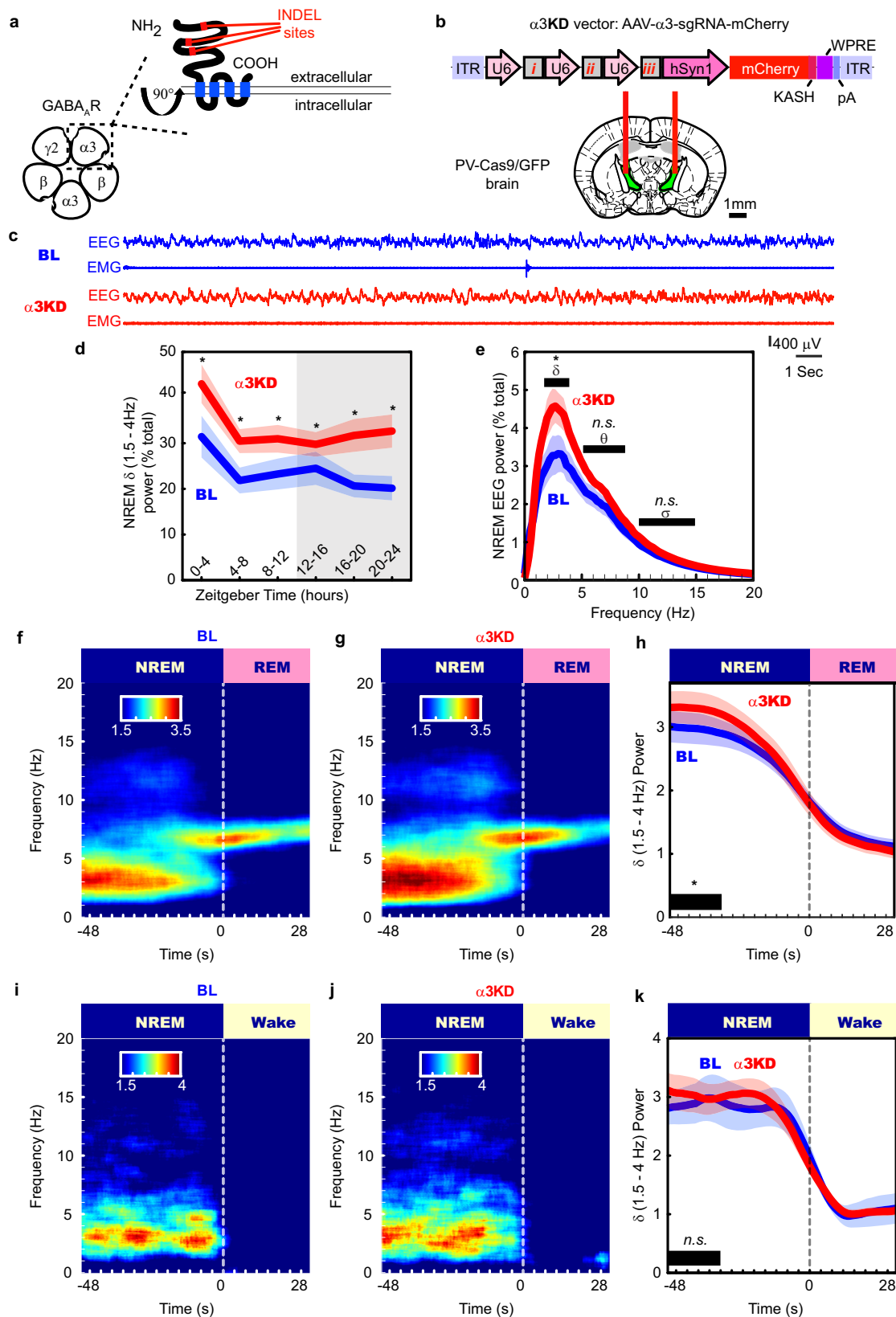
slow wave activity (0.5–4 Hz, which was most pronounced at the beginning of the mouse sleep period (ZT0–4, 47.5 ± 21.8% change, $t(5) = -5.159$, $p = 0.0036$). The increase in slow wave activity was similar in magnitude to the increase observed in the first four hours following six hours of sleep deprivation²⁸, even though the mice here were not sleep deprived.

The 0.5–4 Hz EEG band includes both cortically-generated slow waves (typically 0.5–1 Hz or 0.5–1.5 Hz)^{29–32} and delta oscillations (1.5–4 Hz), which are largely thalamically generated^{29–32}. More fine-grained analysis of our data to separate out these two components revealed that significant increases were seen in the 1.5–4 Hz delta range (Fig. 1d, e and Supplementary Fig. 1) as well as in narrower bands including the delta2 (2.5–3.5 Hz) band which is sensitive to sleep deprivation³¹ (Supplementary Table 1) whereas there was no significant change in slow oscillation (0.5–1.5 Hz, 0–1 Hz or 0.5–1.75 Hz) EEG bands (Supplementary Table 1). 6/6 mice with > 85% transduction of TRN PV neurons showed the increase in delta power (Supplementary Fig. 1). We found no significant change in any other frequency bands in NREM (Fig. 1e), and no changes in any frequency bands during wakefulness or REM sleep (Supplementary Fig. 2). Only modest changes in the amount of NREM sleep itself were observed, with more NREM only in the first four hours of the dark period when mice are mostly awake. (BL 23.2 ± 2.4% vs KD 32.4 ± 2.8%, $t(5) = -4.7472$, $p = 0.005$). Moreover, we found no changes in the duration or frequency of NREM bouts (Fig. 2a). However, we observed a significant reduction in the proportion of shortest bout durations (Fig. 2c), suggesting more consolidated NREM sleep following α3KD. REM sleep was unchanged [duration: BL = 35(1) vs α3KD = 38(3.79); bouts/hour: BL = 6.59(0.41) vs α3KD = 6.42(0.59)]. Analysis of sleep spindles using a recently validated algorithm³³ did not identify any difference in spindle density, frequency or duration (Supplementary Fig. 3). No NREM delta effects were observed in four negative control mice three of which showed no AAV-α3-sgRNA-mCherry transduction in TRN and one with only 66% transduction of TRN PV neurons (Supplementary Fig. 4).

In humans, delta oscillations are most prominent in the deepest stage of NREM sleep, N3. However, in mice NREM is not generally split into stages. Nevertheless, mouse NREM probably also has degrees of depth which are not evident using standard scoring approaches. In humans, arousal threshold increases with depth of NREM sleep; humans are more likely to awaken from the lighter stages N1 or N2³⁴. Thus, we analyzed delta oscillations prior to NREM → REM and NREM → wakefulness transitions. The heightened delta power associated with α3KD was only evident during NREM sleep preceding transitions to REM sleep (Fig. 1f–h) [means (standard error (SEM)): BL = 2.98 (0.24), α3KD = 3.3 (0.26); 11.5% change for all transitions occurring during the light period (±5.56); $t(5) = 2.14$, $p = 0.04$]. No difference was apparent in NREM sleep before transitions to wake (Fig. 1i–k). Similarly, no change in delta power was seen during NREM sleep in the initial phase of transitions from wakefulness to NREM sleep (Supplementary Fig. 5). We also found that increased delta power prior to NREM → REM transitions was not apparent in the negative control group with either no or poor TRN targeting (Supplementary Fig. 4).

Enhanced NREM delta corresponds to longer NREM bouts.

Sleep is more fragmented in mice than in humans. Thus, we reasoned that long NREM bouts might be required to observe large increases in delta. Further analysis of NREM-REM transitions revealed larger increases in delta power within sustained NREM periods prior to transitions to REM (Fig. 3a). Interestingly, heightened delta was seen at the onset and throughout the NREM bout, rather than gradually increasing as a NREM bout persists (Fig. 3a). Delta power levels were higher in longer NREM



bouts and were increased more by the $\alpha 3$ KD. In fact, there was a highly significant linear relationship whereby the longer the NREM duration preceding a NREM-REM transition, the larger the increase in delta power, as measured by percent changes (Fig. 3b). These data also suggested the possibility that the difference in the delta increase observed between NREM-REM and

NREM-wake transitions might be explained, at least in part, by a shorter NREM episode duration prior to NREM-wake transitions compared with the longer NREM preceding REM sleep. This prediction was confirmed since NREM episodes leading to wakefulness were shorter (76.3 ± 7.1 s) than those which transitioned into REM sleep (253.2 ± 30.9 s).

Fig. 1 α 3KD in PV + TRN neurons increased NREM 1.5–4 Hz delta power, especially at NREM to REM transitions. **a** The γ -amino butyric acid receptor type-A (GABA_AR) is a pentameric heteromeric ion channel. CRISPR-Cas9 abscission was directed to three locations (insertion/deletion; INDEL sites) of the gene which correspond to the large extracellular region of the α 3 subunit, a necessary structural as well as ligand binding component in GABA_ARs of the TRN. **b** Adeno-Associated Viral (AAV) vectors encoding three separate single-guide RNAs (*i, ii & iii*), each driven by its own U6 promoter, and the marker protein mCherry driven by the human synapsin (hSyn1) promoter, were injected into the TRN region of PV-Cas9/GFP mice in vivo via guide cannulas. [Adapted from Franklin and Paxinos⁵⁹, with permission from Elsevier]. **c** Examples of frontal electroencephalogram (EEG) and electromyogram (EMG) recordings during a NREM period (ZT0–4) in baseline (BL; blue) and following α 3KD (red), in a single mouse. Panels **d–k** present grand average data from all 6 α 3KD mice. **d** Compared with their baseline (BL) recordings, α 3KD mice had higher non-rapid eye movement sleep (NREM) delta (δ , 1.5–4 Hz) power. ZT0–4, $p = 0.0176$; ZT4–8, $p = 0.0355$; ZT8–12, $p = 0.0335$; ZT12–16, $p = 0.0388$; ZT16–20, $p = 0.0275$; ZT20–24, $p = 0.0221$. Significance was determined using two-tailed paired *t*-tests with Hommel corrected *p*-values. Thick lines indicate mean; envelopes indicate SEM. The shaded area indicates the 12 h dark period. **e** Only NREM delta (δ , 1.5–4 Hz) power is significantly different between BL and α 3KD records ($p = 0.0035$, two-tailed paired *t* test), slow waves (0.5–1.5 Hz), theta (θ , 5–9 Hz) and sigma (σ , 10–15 Hz) power were not affected. The power profile from NREM in ZT0–4 is shown here, the time period where we saw the largest effect. Significance was determined using two-tailed paired *t*-tests. Thick lines indicate mean; envelopes indicate SEM. **f** Baseline time-frequency power dynamics presents high delta power in NREM leading to a transition to rapid eye movement sleep (REM; data from the whole 12 h light period). **g** After α 3KD, the high delta in NREM before a transition to REM was increased. **h** Compared with their BL levels (blue), α 3KD mice (red) had higher delta power in the NREM before a transition to REM [$t(5) = 2.14$, $p = 0.04$]. Significance was tested using a one-tailed paired *t*-test. Thick lines indicate mean; envelopes indicate SEM. **i** BL time-frequency power dynamics presents high delta power in NREM leading to a transition to wake as well. **j** α 3KD did not increase this delta power that occurs during NREM before a transition to wake. **k** Compared with BL (blue), α 3KD (red) did not lead to a change in delta power in the NREM before a transition to wake [$t(5) = 0.23$, $p = 0.41$]. Significance was tested using a one-tailed paired *t*-test. Thick lines indicate mean; envelopes indicate SEM. * $p < 0.05$, n.s. indicates not significant. Color scales represent normalized power (power at time/power from wakefulness).

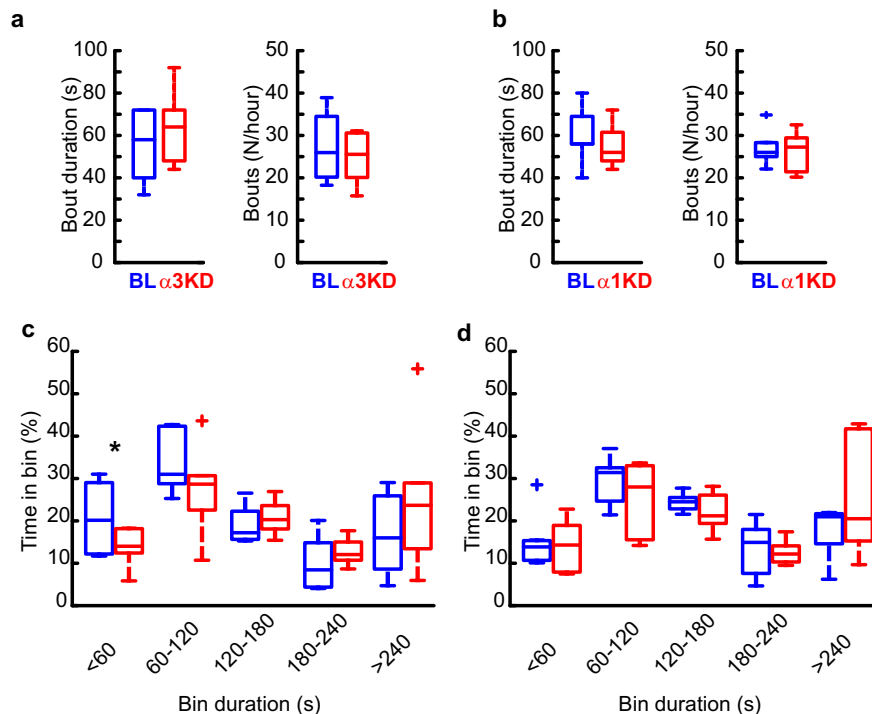
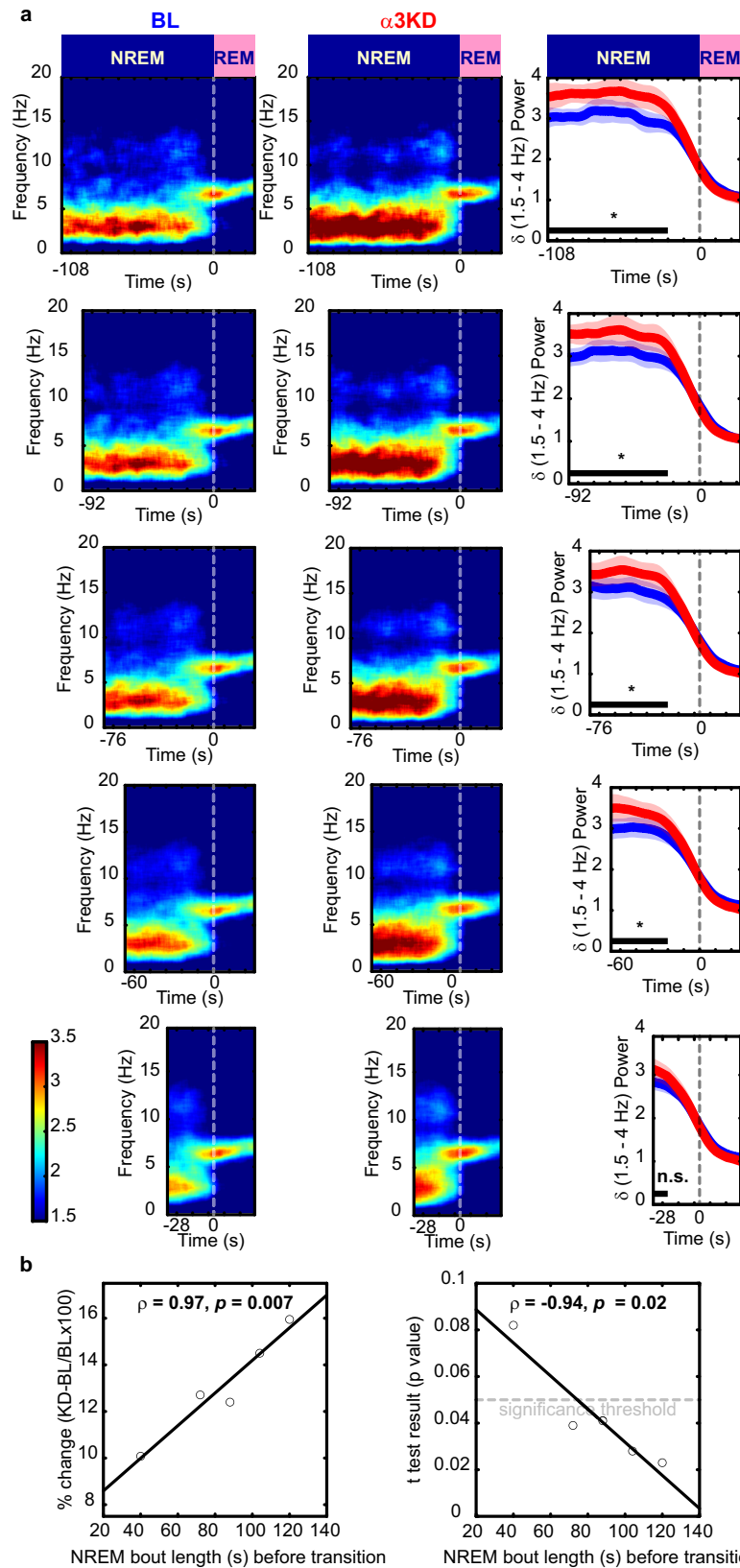


Fig. 2 α 3KD, but not α 1KD, in PV + TRN neurons decreased time spent in the shortest (<60 s) NREM bouts. **a** Compared with their baseline conditions (BL; blue), α 3KD (red) mice ($n = 6$) did not have altered durations or number of NREM bouts. **b** α 1KD mice ($n = 7$) also did not have altered durations or number of NREM bouts. **c** The proportion of time spent in short bouts lasting <60 s was significantly reduced in α 3KD mice (two-tailed paired *t*-test, * $p = 0.03$), but no other bins showed any differences between BL and α 3KD ($n = 6$). **d** The proportion of time spent in bouts was unchanged in α 1KD mice ($n = 7$). Box plots: center lines represent median values, 75th percentiles are box tops and 25th percentiles are box bottoms. + symbols represent outliers defined as >1.5x the interquartile range away from box tops or bottoms. Data from whole 12 h light period.

Widespread α 3KD in TRN determines elevated NREM delta power. Selective deletion of α 3 subunits in TRN PV neurons requires the combination of selective expression of Cas9 in PV neurons and sgRNA targeting α 3 subunits in the same cells. mCherry (red; marker of sgRNA) was expressed in the majority of TRN PV neurons (green) within the core of the injection site (Fig. 4a). In the six α 3KD-confirmed mice, we found a high percentage of PV + TRN neurons (GFP+) were transduced by AAV- α 3-sgRNA-mCherry (mCherry+: $93.9 \pm 2.0\%$), and a large

proportion of the TRN ($94.4 \pm 1.0\%$) area was covered (Fig. 4a; Supplementary Table 2). Analysis of off-target viral spread assessed by mCherry+ cells which were also GFP+ revealed only 5% medially and 3.9% laterally. All cases of off-target mCherry/GFP colocalization were found exclusively in the anterior dorsal thalamic nucleus and globus pallidus (Supplementary Table 3). Neither of these regions express substantial amounts of α 3 subunit containing GABA_A receptors^{35–39}. Thus, our functional effects are highly likely to be due to effects on the TRN. In



preliminary work prior to in vivo experiments, we confirmed that Cas9 expression (marked by GFP co-expression) was selective for PV neurons by immunohistochemical staining for PV (Fig. 4b), consistent with the previously published validation of Cas9 selective expression in PV+ neurons in this mouse model⁴⁰.

α 3KD causes a functional ablation of sIPSCs in TRN neurons. In a separate group of mice, we verified a functional ablation of GABA_A receptors in whole-cell patch-clamp recordings from TRN PV neurons in vitro. Recordings were performed from adult mice (>2.5 months). In contrast to earlier in development⁴¹, at this age in

Fig. 3 α 3KD caused the largest delta (δ , 1.5–4 Hz) effect in the longest NREM bouts before REM. **a** Analysis of non-rapid eye movement sleep (NREM) to rapid eye movement sleep (REM) transitions reveals larger delta power increases in longer NREM episodes, baseline (BL; blue) vs α 3KD (red). Periods with stable delta (black bars), were tested for significance (one-tailed paired *t*-tests, **p* < 0.05, n.s. not significant; *p*-values: 0.023; 0.028; 0.041; 0.039; 0.082.). The 24 s prior to NREM-REM transitions, when delta decays, were not included in statistical analyses. **b** Percent change in NREM delta power was positively correlated with NREM bout length prior to REM. *P* values from *t*-tests (BL vs α 3KD) were negatively correlated with NREM bout length prior to REM as determined using Pearson's linear correlation, two-tailed, ρ is Pearson's linear correlation coefficient. Data from 12 h light period. *N* = 6. Color scales represent normalized power (power at time/power from wakefulness).

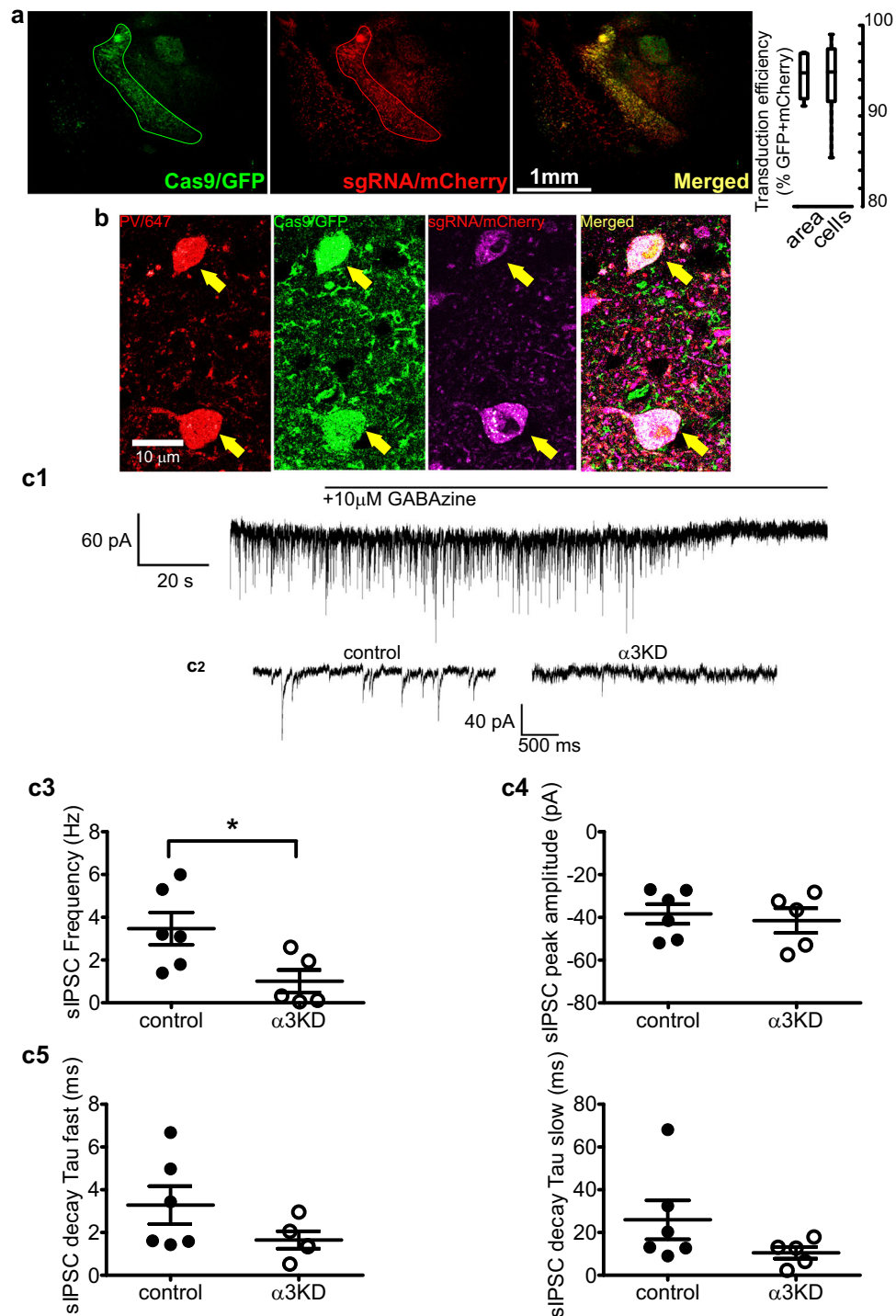


Fig. 4 α 3KD in PV + TRN neurons was validated by histology and in vitro electrophysiology. **a** GFP indicates rich Cas9 expression within the TRN region (green outline), TRN projections to thalamocortical nuclei and sparse distal expression in the globus pallidus (GP). mCherry reveals widespread transduction of the TRN region by the AAV vector delivering sgRNAs (red) with many of the cells in the area co-expressing both markers (merged; yellow). Percentages of target cells and target area that co-express markers reveal widespread delivery of sgRNAs to target TRN PV neurons in the mice used for in vivo studies. Further quantification of transduction is given in Supplementary Tables 2 and 3. Box plots: center lines represent median values, 75th percentiles are box tops and 25th percentiles are box bottoms, bars represent maximum and minimum. ($n = 6$). **b** High magnification (60x) confocal images show triple co-localization of PV (immunohistochemical stain; red), Cas9 (GFP; green), and sgRNA (viral transduction indicated by mCherry; magenta), demonstrating successful targeting of PV + neurons within the TRN. Micrographs are representative of $n = 2$. **c1** Inward-going spontaneous inhibitory postsynaptic currents (sIPSCs) recorded from TRN PV neurons using a high chloride intracellular solution in the presence of ionotropic glutamate receptor antagonists are blocked by the selective GABA_A receptor antagonist, GABA_Azine (10 μ M). **c2** Compared with PV + TRN neurons without KD (control), sIPSCs in α 3KD PV + TRN neurons were reduced (α 3KD). **c3** Compared with control recordings from PV + TRN neurons without KD (left), the frequency of sIPSCs in α 3KD PV + TRN neurons was significantly reduced (right). * $p = 0.031$, unpaired two-tailed t -test. **c4, 5** Compared with control recordings from PV + TRN neurons without KD, residual sIPSCs in α 3KD PV + TRN neurons (right) had unaltered amplitude (**c4**) or decay time constants (**c5**). **c3–c5** broad lines indicate means, error bars represent SEM control: $n = 6$; α 3KD $n = 5$.

mice there is little evidence for functional intra-TRN chemical synapses^{41,42}. Thus, the GABA_A receptor mediated events we record in TRN PV neurons likely arise from extra-TRN inputs arising in the basal forebrain, lateral hypothalamus and globus pallidus^{20,21,43}. In control voltage-clamp recordings from TRN PV neurons held at -70 mV in PV-tdTomato mice (which serve as wild type controls with a visual marker of the correct cell phenotype), spontaneous inhibitory postsynaptic currents (sIPSCs) were observed in the presence of glutamate receptor antagonists (20 μ M 6-cyano-7-nitroquinoxaline-2,3-dione + 50 μ M D-(2R)-amino-5-phosphonopentanoic acid) and were abolished by a GABA_A receptor antagonist, GABA_Azine (10 μ M) (Fig. 4c1). To enhance the driving force for chloride, recordings were made using a patch solution with a high chloride concentration. Thus, IPSCs were detected as inward currents (Fig. 4c1, 4c2). In PV-Cas9 mice, the frequency of sIPSCs were significantly reduced in recordings from green (PV-Cas9/GFP) and red (transduced with AAV- α 3-sgRNA-mCherry) fluorescent TRN neurons one month post-injection, whereas the amplitude was unaltered [Frequency: PV-tdTomato: 3.47 ± 0.75 Hz ($N = 6$ from four animals); PV-Cas9+AAV- α 3-sgRNA: 1.01 ± 0.53 ($N = 5$ from four animals); $t(9) = 2.560$, $p = 0.031$, t -test, (Fig. 4c3). Amplitude: PV-tdTomato: -38.4 ± 4.6 pA ($N = 6$); PV-Cas9+AAV- α 3-sgRNA: -41.5 ± 5.8 pA ($N = 5$), $t(7) = 0.4426$, $p = 0.6793$, t -test; (Fig. 4c4). The bi-exponential decay of residual sIPSCs in PV + TRN neurons in PV-Cas9 mice with α 3KD was not significantly different from that in control PV-tdTomato mice [Fig. 4c5; Fast decay time constant: PV-tdTomato 3.29 ± 0.89 ms; PV-Cas9+AAV- α 3-sgRNA: 1.64 ± 0.41 ($N = 5$), $p = 0.1524$, t -test. Slow decay time constant: PV-tdTomato 26.0 ± 9.1 ms; PV-Cas9+AAV- α 3-sgRNA: 10.6 ± 2.7 ($N = 5$), $p = 0.1692$, t -test]. Furthermore, residual sIPSCs retained sensitivity to an α 3 selective positive allosteric modulator, TP003 [1 μ M TP003, slow component of bi-exponential decay time increased by $19.2 \pm 6.5\%$, $p = 0.071$, $N = 3$, paired t -test], suggesting that other α subunits were not upregulated in response to the α 3KD. No change was observed in the holding current (PV-tdTomato control: -141.0 ± 26.0 pA; PV-Cas9+AAV- α 3-sgRNA -84.4 ± 7.6 pA, $p = 0.1155$) indicating that knockdown of α 3 subunits did not alter the passive membrane properties of TRN PV neurons.

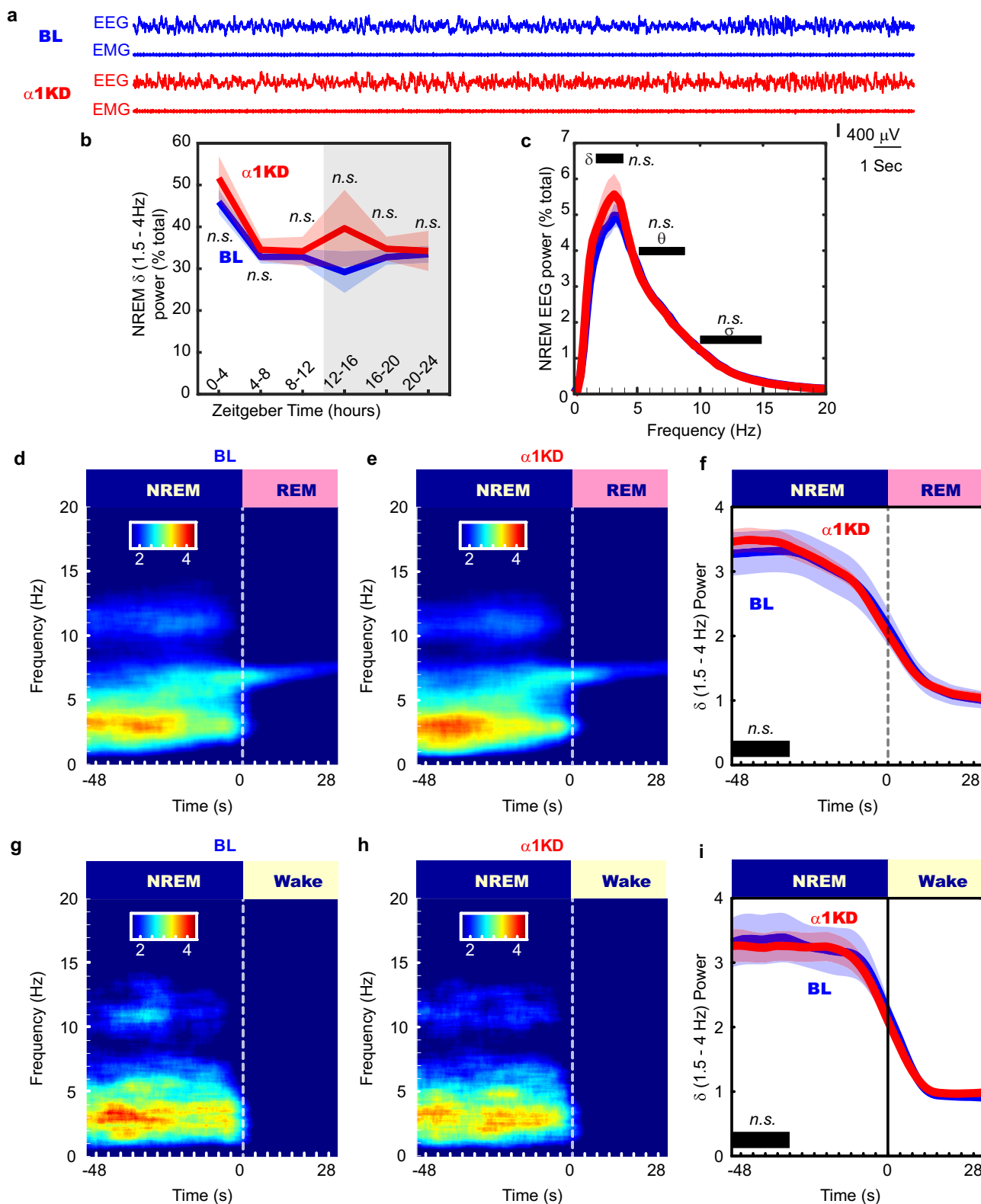
No effect by control α 1KD. In another group of mice, we performed the same in vivo experimental protocol with a control AAV vector targeting the GABA_AR α 1 subunit. The TRN is devoid of α 1 subunits, so this experiment controls for non-specific genetic cutting. In these mice ($n = 7$), we found no change in the amount of NREM delta power (Fig. 5a, b), or other bands in NREM (Fig. 5c) following the α 1KD. No frequency bands of wakefulness or REM sleep were altered either. The time-frequency analysis at NREM-REM transitions (Fig. 5d–f) and at NREM-Wake transitions (Fig. 5g–i) showed no changes. There

were also no changes to the duration or frequency of NREM bouts (Fig. 2b), or the proportions of bout durations (Fig. 2d). Our histologic protocol confirmed a similar degree of targeting success (Supplementary Fig. 6) as in the α 3KD.

Discussion

In this study, we used cell-type and region-specific CRISPR-Cas9 gene editing in vivo to test the functional role of GABAergic inhibition onto TRN neurons in controlling sleep physiology. We found that knockdown of α 3-containing GABA receptors, confirmed using in vitro recording of sIPSCs, selectively enhances the power of NREM delta oscillations during the sleep period of mice. Further analyses identified long NREM episodes prior to NREM-REM transitions as being particularly strongly affected by α 3KD. The selectivity of our manipulations was confirmed by control experiments with absent or low transduction and experiments targeting a closely related subunit, α 1, which is not expressed by TRN neurons.

There is an emerging consensus that depolarization of TRN neurons during NREM is an effective way to promote deep sleep^{17–23}. TRN neurons receive GABAergic inputs from basal forebrain, lateral hypothalamus and globus pallidus, and several of these neuronal groups maintain a high discharge rate during NREM sleep^{20,21,43}. Previous in vitro work⁴⁴ showed that disinhibition of TRN neurons via local pharmacological blockade of GABA_A receptors in TRN enhances GABAergic inhibition in thalamocortical neurons. Thus, withdrawal of these inputs by removing their postsynaptic targets will lead to a higher discharge rate of TRN neurons during NREM sleep, particularly during deeper stages of NREM prior to REM sleep when excitatory inputs from brainstem aminergic cell groups wane. In turn, increased activity of TRN GABAergic neurons will lead to hyperpolarization of thalamocortical relay neurons, bringing their membrane potential into the correct range to generate delta oscillations. This interpretation of our results is consistent with previous work which suggested that modulating the polarization level and discharge rate of TRN neurons affects delta oscillations and NREM sleep^{17–22}. In particular, tonic optogenetic excitation of TRN neurons increased burst discharge of thalamocortical relay neurons at delta frequencies and increased cortical delta power¹⁷. Taken together, our in vitro electrophysiology experiments and the prior literature suggest that the increase in cortical delta power in our experiments is likely explained by increased tonic discharge of TRN PV neurons due to reduced extra-TRN inhibitory influences and enhanced delta-frequency bursting of thalamocortical neurons. We also note that reduced burst discharge of TRN neurons due to knockout of Cav3.3 channels or chemogenetic inhibition of TRN neurons can lead to increased delta power²³ but in contrast to the results reported here and in previous studies^{17–19}, these manipulations reduce the power of slow oscillations and sleep spindles²³. Given



the functional importance of slow oscillations and sleep spindles, manipulations which increase TRN activity during sleep may be more beneficial than those which reduce burst discharge or cause strong hyperpolarization.

Our findings differ from previous work which examined constitutive global $\alpha 3$ subunit knockout (KO) mice^{25,45}. In the constitutive KO there was no reduction in sIPSC frequency compared to controls in TRN neurons; in fact, there was a modest

increase in frequency, plus a significant increase in amplitude and alterations in kinetics and pharmacology, suggesting developmental compensation. Conversely, we show a significant reduction in sIPSC frequency. Here, the ablation was performed in the adult brain, so developmental compensation was circumvented, which is evident by the lack of change in the amplitude of residual IPSCs or their decay time constant, as well as the fact that residual sIPSCs retained sensitivity to an $\alpha 3$ selective positive allosteric

Fig. 5 The control cohort with $\alpha 1$ KD in PV + TRN neurons displayed no changes to NREM or wake time, or delta (δ , 1.5–4 Hz) power in any states, including transitions from NREM to REM, in the light (inactive) period. **a** Examples of frontal electroencephalogram (EEG) and electromyogram (EMG) recordings during a NREM period (ZT0–4) in baseline (BL; blue) and following $\alpha 1$ KD (red), from a single mouse. **b** Compared with their baseline (BL) recordings, $\alpha 1$ KD mice had unchanged non-rapid eye movement sleep (NREM delta power ZT0–4, $p = 0.2$; ZT4–8, $p = 0.32$; ZT8–12, $p = 0.58$; ZT12–16, $p = 0.42$; ZT16–20, $p = 0.47$; ZT20–24, $p = 0.88$). Significance was determined using two-tailed paired t -tests. Thick lines indicate mean; envelopes indicate SEM. The shaded area indicates the 12 h dark period. **c** NREM delta (δ) theta (θ) and sigma (σ) power were not different between BL and $\alpha 1$ KD records, shown here is the power profile from NREM in ZT0–4 when we saw the largest effect in the $\alpha 3$ KD mice. Significance was determined using two-tailed paired t -tests. Thick lines indicate mean; envelopes indicate SEM. **d** Baseline time-frequency power dynamics reveal high delta power in NREM leading to a transition to rapid eye movement (REM) sleep. **e** After $\alpha 1$ KD, the high delta power in NREM before a transition to REM is the same as in baseline records. **f** Compared with baseline (blue), $\alpha 1$ KD (red) mice had unaltered delta power in the NREM before a transition to REM [$t(6) = 0.67$, $p = 0.26$]. Significance was tested using a one-tailed paired t -test. Thick lines indicate mean; envelopes indicate SEM. **g** Baseline time-frequency power dynamics reveals high delta power in NREM leading to a transition to wake. **h** $\alpha 1$ KD did not increase the delta in NREM before a transition to wake. **i** Compared with baseline (blue), $\alpha 1$ KD (red) mice had unchanged delta power in the NREM before a transition to wake [$t(6) = -0.36$, $p = 0.63$]. Significance was tested using a one-tailed paired t -test. Thick lines indicate mean; envelopes indicate SEM. *n.s.* indicates not significant. **d–i** show data from whole 12 period of light. **b–i** $N = 7$. Color scales represent normalized power (power at time/power from wakefulness).

modulator. Therefore, functional ablation of $\alpha 3$ subunits in adults was feasible with the CRISPR-Cas9 approach and, importantly, allowed us to unravel the role of the $\alpha 3$ subunits in sleep-wake patterns and EEG profiles. Despite marked changes in GABAergic transmission in the TRN in the constitutive global $\alpha 3$ knockout, there was no change in the intrinsic membrane properties of TRN neurons or in the properties of glutamatergic inputs from thalamocortical relay neurons^{25,45}. Similarly, we found no change in the holding current of TRN PV neurons in vitro. Thus, alterations in GABAergic transmission in TRN do not appear to lead to compensatory alterations in the thalamocortical circuitry which generates delta oscillations.

In conclusion, CRISPR-Cas9 cell and region-specific gene editing of $\alpha 3$ subunits in adult mice identified a functional role of GABA_A receptors on TRN PV neurons in regulating deep NREM sleep. Pharmacological agents which allosterically increase the activity of GABA_A receptors containing the $\alpha 1$ or $\alpha 3$ subunits are widely used hypnotics. Unfortunately, they promote light sleep with reduced delta power^{9,10,46}. Our results suggest that the delta suppressing effect of z-drugs may come from potentiating the $\alpha 3$ containing GABA_ARs of the TRN (i.e., the opposite effect that we report here; $\alpha 3$ KD leads to increased delta power), a sleep-regulating region which has one of the highest densities of $\alpha 3$ subunits in the brain. Clinically, this is a problem because high NREM delta waves of deep sleep are restorative, important for memory consolidation⁴⁷ and clearance of toxic metabolites³. Here knockdown of $\alpha 3$ subunits on TRN neurons enhanced deep sleep while not negatively affecting other sleep oscillations or wake power spectra. Mainstay sleep medicines which potentiate GABA_A receptors, termed z-drugs, suppress delta waves. Each drug preferentially targets various isoforms. For example, Zolpidem and eszopiclone both bind to $\alpha 1$ $\alpha 2$ and $\alpha 3$, eszopiclone additionally binding $\alpha 5$ ⁴⁸. Interestingly GF-015535-00, not currently approved for clinical use, is highly selective for $\alpha 1$ and causes far less delta suppression than currently approved z-drugs⁴⁹. An ideal next-generation hypnotic agent may sedate by positive allosteric modulation of $\alpha 1$ subunits (as with conventional z-drugs); but simultaneously boost delta waves by negatively modulating $\alpha 3$ subunits which are highly expressed in TRN of humans/primates^{50,51}, as well as mice. This mechanism could enhance the properties of natural restorative delta oscillations of NREM sleep in manner that current hypnotics do not.

Methods

Mice. To target our Clustered Regularly Interspersed Short Palindromic Repeats Knock Down (CRISPR KD) selectively to the major subset of Thalamic Reticular Nucleus (TRN) neurons which express Parvalbumin (PV) we crossed male Rosa26-lox-stop-lox-Cas9/GFP (Jackson Labs stock # 026175) mice with female PV-Cre (Jackson Labs stock # 017320) mice, generating mice with the key CRISPR enzyme

Cas9 and a green fluorescent protein (GFP) reporter expressed selectively in PV neurons, PV-Cas9/GFP mice. For one control group used for in vitro sIPSCs recordings, we used PV-tdTomato mice generated by crossing male Rosa26-lox-stop-lox-tdTomato (Jackson Labs stock # 007914) mice with female PV-Cre mice. 3–8 month-old mice of both sexes were used for in vivo and in vitro experiments. No obvious sex differences were observed so data were pooled. Mice were housed with a 12 h:12 h light:dark cycle with lights on at 7am, at ambient temperatures 26–34 °C and 30–70% humidity. Food and water were available ad libitum. All experiments were approved by the Institutional Animal Care and Use Committee of VA Boston Healthcare System and conformed to National Institute of Health, Veterans Administration and Harvard Medical School guidelines. The work was carried out under protocols 236-B-042916, 359-B-041618 & 400-W-110419.

Adeno-associated viral (AAV) vectors. For this study, the PX552 plasmid described and validated by Swiech et al.⁵² (Addgene plasmid # 60958; <http://n2t.net/addgene:60958>; RRID:Addgene_60958) was modified to encode triple U6-sgRNA cassettes each targeting a distinct locus of the target genes. The GFP sequence was replaced by the sequence encoding the red fluorescent protein, mCherry, since GFP was already expressed in PV neurons in the PV-Cas9/GFP mice used for experiments. This custom plasmid became our backbone for sub-sequent design of our control vector.

AAV- $\alpha 3$ -sgRNA-mCherry. To selectively inactivate the gene encoding the only $\alpha 3$ subunit ($\alpha 3$) of GABA_A receptors expressed in TRN²⁶, we used the above custom-designed AAV vector to deliver three sgRNAs targeting the gene encoding the $\alpha 3$ GABA_A subunit (*Gabra3*) within the TRN: (*Gabra3*; NCBI Reference Sequence: NM_008067.4): *i*: 5' TCTTACTAGAAATCTTGGAT 3' *ii*: 5' GGACCCTCTC TATACAATG 3' and *iii* 5' TTGTTGGGACAGAGATAATC 3'. We found in silico that the $\alpha 3$ -sgRNAs had no off-targets in the mouse genome⁵³. The CRISPR design tools <http://crispr.mit.edu/> and <http://chopchop.cbu.uib.no/>⁵⁴ were used to aid initial identification of possible sgRNA sequences corresponding to the N-terminal domain (Fig. 1a). The sgRNA candidate sequences were manually selected by alignment analysis (Bioedit; open-source software, Ibis Therapeutics, CA) to confirm that they did not target the closely related gene encoding the $\alpha 1$ subunit; (*Gabra1*; NCBI Reference Sequence: NM_010250.5). Though not found in TRN, $\alpha 1$ is present in the thalamus²⁶ and we wanted to avoid off target GABA_A receptor KD, which we viewed as the only tangible confound beyond non-specific CRISPR-Cas9 abscission. All three $\alpha 3$ -sgRNA showed minimal homology with $\alpha 1$ and was not indicated to be an off-target site in silico.

AAV- $\alpha 1$ -sgRNA-mCherry. We designed another vector bearing three sgRNAs targeting the $\alpha 1$ gene of GABA_A receptor. One sgRNA with low homology to $\alpha 3$ but perfect homology to $\alpha 1$ with a PAM sequence and the other two mock-sgRNAs with perfect homology to non-PAM bearing areas of $\alpha 1$ gene were chosen. *i*: 5' CTCAATCTGAGCAGACTGTC 3' *ii*, 5' TTTTCGTCAAAAGTTGGAA 3' *iii* 5' TTGGACAAACAGTTGACTCT 3'. All three sequences from mouse $\alpha 1$ gene showed no off-targets in silico in the mouse genome⁵³. We used snappene software for plasmid design, construction was outsourced to GenScript (New Jersey, United States; www.genscript.com/) and validated by restriction mapping by gel electrophoresis and sequencing. Plasmids, thus validated, were packaged into AAV¹² particles/ml were determined by dot-blot analysis and used for microinjections into the TRN (Fig. 1b).

Stereotaxic surgery and AAV microinjections into TRN. Executing the selective CRISPR KD of $\alpha 3$ subunits in TRN PV neurons requires expression of the sgRNAs targeting $\alpha 3$ subunits combined with the Cas9 expressed in PV neurons of the

transgenic mice. We achieved this combination by stereotaxic injection of the AAVs expressing sgRNAs into the TRN of the PV-Cas9/GFP mice. Using a Kopf stereotaxic frame, we chronically implanted cannulas bilaterally above the anterior TRN (Plastics One; Connecticut, United States), Part # C315G/SPC, total length 12 mm), with retainers inserted (Plastics One, Part # C15I/SPC), at AP -0.7 mm, ML ± 1.4 , DV -1.5 . The coordinates for cannula location were selected to be 2 mm above the TRN to allow subsequent microinjection into TRN without extensive damage to TRN. We targeted anterior TRN since anterior TRN neurons project to thalamocortical regions which innervate anterior cortex where our EEG recording electrode was located⁵⁵. To record cortical electrical activity, bilateral frontal neocortical EEG screw electrodes (Pinnacle Technology Inc.; Kansas, United States; Part # 8403) were placed at AP $+1.9$ mm, ML ± 1.5 with a reference electrode at AP -3 mm, ML $+2.7$ and a ground electrode at AP -6 mm ML $= 0$ respectively and soldered to a headmount (Pinnacle Technology Inc.; Part # 8201-SS). EMG electrodes were placed in the nuchal muscle. All the chronically implanted components were secured with dental cement (Keystone industries, Bosworth Fastray; Part # 0921378).

Following one full week of recovery from cannula/electrode implantation, and collection of baseline EEG/EMG records (see next section), AAV microinjections were made into the TRN. Mice were anesthetized by isoflurane (1.5–4% in O₂) and depth of anesthesia was monitored by breathing rate, pedal withdrawal and tail pinch reflexes. A 5 μ l Hamilton syringe (Part # 87908, Model 75 SN SYR with 33 g cemented needle) loaded with viral solutions was lowered through the cannula, 2 mm beyond the cannula tip, into the TRN (DV -3.5). 1 μ l microinjections were delivered at 0.05 μ l/minute using a micropump (KD Scientific Legato 130, Massachusetts, United States). Doses of Meloxicam (5 mg/kg; intraperitoneal) were given immediately after surgery and again 22–24 h later, to mitigate any pain associated with the surgery. One month following AAV injection, EEG/EMG signals were again recorded and compared to baseline recordings.

Electroencephalogram (EEG)/Electromyogram (EMG) recordings. To study sleep wake-states and thalamocortical oscillations, we recorded EEG and EMG using Pinnacle Technology Inc. 3 channel (2 EEG/1EMG) systems for mice (Part # 8200-K1-SL), using its acquisition software (Sirenia Acquisition). Mice were tethered to the system via mouse pre-amplifiers (Pinnacle Technology Inc. Part # 8202-SL) and 24-hour recordings were collected between zeitgeber time 0–24 following a 48-hour period of habituation to the recording apparatus. EEG/EMG data was sampled at 2 kHz, amplified 100x and low pass filtered at 600 Hz. In one mouse from the α 3KD cohort and one mouse from the control cohort which lacked transduction of PV + TRN neurons, we missed data from ZT0–ZT2. In one mouse from the control cohort which lacked transduction of PV + TRN neurons we missed data from ZT0–ZT3. These were due to software malfunctions. We dealt with this by continuing the recordings into the subsequent day and using the same ZT hours to replace the missing data.

Sleep-wake scoring and EEG analysis. We manually scored sleep-wake states from EEG and EMG records using four second epochs as follows: Wake was scored when EEG showed a desynchronized low amplitude signal with muscle tone evident by a large EMG signal; the large EMG signal did not need to be phasic in appearance to be characterized as wake. NREM sleep was scored when the EEG signal showed large amplitude, slow synchronized waves, and a low EMG signal, except for very brief bursts which were considered twitching. REM sleep was scored when the EEG signal presented a repetitive stereotyped ‘sawtooth’ signal in the theta range (5–9 Hz), with a nearly flat EMG signal. Artifacts were dealt with as follows: periods that appeared to be wakefulness, but the EEG was contaminated by crosstalk with EMG signals, were scored as ‘wake-exclude’. Periods of NREM or REM with large amplitude DC shifts were extremely rare and labeled as ‘NREM-exclude’ or ‘REM-exclude’. We used all epochs, even those marked ‘exclude’, in behavioral analyses such as time in state or bout analysis, but we only included artifact free data for analyses of EEG signals, such as power spectral density or time-frequency analyses. Scoring was performed in Sirenia Sleep, and EEG signals and scored epochs were exported for further analysis in MATLAB.

Power spectral density of wake, NREM and REM was computed using the MATLAB pwelch function using an 4-second Hanning window with 50% overlap. To normalize EEG power, power from each state was normalized to the total power from the entire 24 h record. We used this approach having read methods in previous sleep-wake power analysis in mice⁵⁶. Briefly, delta power dynamics across the 24 h record were binned in 4-hour intervals (still normalized to the full 24 h record) to ensure there were no periods devoid of NREM, all NREM bouts were used to compute NREM delta power. To produce time-frequency spectrograms for state-transition analysis, we first down-sampled the data to 40 Hz and screened for outliers, replacing values more than two standard deviations away from the mean with zeros. We then used the multi-taper method⁵⁷ (Chronux Toolbox; Chronux.org) function (5 tapers with 10 s sliding window in 100 ms steps). Spectra were computed for each state-transition per mouse and mean averaged. Each within-animal mean averaged time-frequency spectrum was then normalized to its average power from wakefulness (I.E. Frequency bin from spectra/Frequency bin from wake). These normalized spectra were then mean averaged across all the animals in the group for a grand mean averaged spectrogram. Mean averaged power in the delta band (1.5–4 Hz) was plotted with standard error envelopes,

smoothed using a 5 s moving average window. We analyzed sleep spindles using our validated automated spindle detection algorithm³³ and plotted them at NREM-REM transitions as mean values of corresponding 12 s periods across all transitions. For bout analysis, bout durations were binned into discrete intervals, summed, and presented as a percentage of total time in the state. We used this approach having read methods in previous sleep-wake bout analysis in mice⁵⁸.

Histology. Mice were transcardially perfused with 10 ml phosphate buffered saline (PBS) followed by 10 ml of 10% formalin for fixation. Brains were extracted and subsequently immersion-fixed in 10% formalin for 1–2 days, followed by 30% sucrose solution in PBS before tissue was sliced at a thickness of 40 μ m on a freezing microtome (Leica Biosystems, Illinois, United States).

We first confirmed previous findings⁴⁰ that Cas9 was expressed selectively in TRN PV neurons, by performing immunohistochemistry for PV in coronal sections containing TRN from PV-Cas9/GFP mice. Free-floating sections in wells were treated with PV primary antibodies sheep anti-PV (1:150; AF-5058; R & D Systems, Minneapolis, MN) and far-red secondary antibodies (donkey anti-sheep IgG conjugated to AlexaFluor 647; 1:250; ab 150179; Abcam, Inc. Waltham, MA). GFP signal was enhanced using mouse anti-GFP antibody (1:300; MAB3580; EMD Millipore, Burlington MA) and the green secondary antibody donkey anti-mouse IgG conjugated to AlexaFluor 488 (1:500; #A-21202; ThermoFisher Scientific, Waltham, MA). Confocal imaging was performed for triple fluorescence (mCherry, AF488, AF647) using 60x oil objective of Leica Dmi8 confocal microscope and LAS X software.

For histological verification of transduction efficiency, sections were mounted on microscope slides and coverslipped using Vectashield Hard Set mounting medium (Part # H-1400, Vector Labor). Images were collected on a Zeiss Image2 microscope, outfitted with a Hamamatsu Orca R2 camera (C10600) and Stereo Investigator software (MBF Bioscience). For our in vivo sleep-wake experiments, we visually confirmed the presence and quantified co-expression of sgRNAs and Cas9 within TRN by identifying fluorescent markers of sgRNAs (mCherry) and Cas9 (GFP). GFP+ neurons were identified by green fluorescence in the cytoplasm (excitation:emission 488:509) and mCherry+ neurons were identified by red fluorescence in the cytoplasm (excitation:emission 590:617).

For measures of transduction success, we calculated percentages of targets based on an average of two sections per brain. mCherry signals marking AAV transduction were consistently found within the anterior-posterior location, Bregma -0.8 ± 0.2 mm. Target areas were measured using the Fiji free-hand tool (<https://imagej.net/Fiji>) which reports a manually drawn area in pixels. We first drew an area around the GFP+ TRN region; within this, we drew a second area which was mCherry+. Percentages reported represent the percent of the mCherry+ area divided by the total GFP+ area. Targeted cells were counted manually using the Fiji multipoint tool. We first counted all the GFP+ cells within the TRN region, then we counted all the cells that were both mCherry+ and GFP+ within that region. Percentages represent the number of double labeled (mCherry+GFP+) cells divided by total number of GFP+ cells within the TRN. Mice were considered successful cases if any TRN region was found to be positive for both mCherry and GFP. All successful cases were used to quantify transduction, as described above. In three cases, no signal for mCherry was found within the GFP+ TRN region and were excluded from the cohort, in one mouse transduction efficiency was 63.5% (area) and 66.4% (cells). The in vivo data from these four mice were used only in the serendipitous control cohort of Supplementary Fig. S4.

In vitro slice electrophysiology. Adult (3–8 Month) mice were deeply anesthetized with isoflurane and decapitated at ZT4–5. To knockdown α 3 subunits in TRN, mice were injected at 2.5 Months and slices were prepared 4–5 weeks later. Coronal brain sections containing TRN (Bregma -0.46 to -0.94 mm) were cut at 300 μ m-thickness with a Leica VT1200S vibratome (Leica Biosystems Inc., Buffalo Grove, IL, USA) at 4 °C. After slicing, the slices were placed into ACSF containing the following (in mM): 124 NaCl, 1.8 KCl, 25.6 NaHCO₃, 1.2 KH₂PO₄, 2 CaCl₂, 1.3 MgSO₄, and 10 glucose (300 mOsm), saturated with 95% O₂/5% CO₂ for at least 1 h at room temperature before being transferred to the recording chamber and superfused with warm ACSF (32 °C) at 2–3 ml/min.

Spontaneous inhibitory post-synaptic current (sIPSC) recordings focused on the anterior-dorsal section of the TRN and target cells were identified by GFP expression and mCherry expression. We filled 3–6 M Ω patch pipettes with intracellular solution of the following composition (in mM): 130 KCl, 5 NaCl, 2 MgCl₂, 10 HEPES, 0.1 EGTA, 2 Na₂ATP, 0.5 NaGTP, 4 MgATP and 1 spermine, pH 7.25 with KOH (280 mOsm). sIPSCs were recorded at -70 mV in the presence of the glutamate receptor antagonists (20 μ M 6-cyano-7-nitroquinoxaline-2,3-dione +50 μ M D-(2R)-amino-5-phosphonopentanoic acid) using a Multiclamp 700B amplifier and pClamp 10.0 software (Molecular devices; California, United States). A 1 min period after 5 min application of the glutamate receptor antagonists was used for statistical analysis. Only well resolved events with amplitudes >10 pA were analyzed (Igor Pro6.02A, WaveMetrics, Inc., Portland, OR, USA). To analyze the decay of sIPSCs, in clampfit 10.2 software (Molecular Devices, LLC, San Jose, CA, USA), each sIPSCs event was detected and normalized according to its negative peak (range of 0.3 ms around the peak). An averaged trace for each cell was then generated by averaging the normalized events. The peak-to-baseline phase of the averaged trace was fitted with a two-term exponential function in GraphPad prism5 (GraphPad Software, San Diego, CA, USA). Series resistance was 6–20 M Ω

and was not compensated. Sampling rate was 20 kHz. Records were low-pass (Bessel) filtered at 1 KHz.

Statistics. We used a Jarque–Bera test to evaluate data distribution before choosing an appropriate inferential test. Normality was never violated and parametric tests were used uniformly. Multiple two-tailed paired *t*-tests were used to compare BL vs KD areas under delta power or other defined frequency bands (represented by bold black lines and symbols δ , θ or σ ; ‘significant’ or ‘not significant’ is indicated by * or *n.s.* respectively) in NREM, wake or REM. We used Hommel corrected *p*-values to account for family-wise error rates to report significance. We found a unidirectional effect on NREM delta, so we used a one-tailed test in subsequent delta power analyses, comparing areas under dynamic changes in delta power at state-transitions (also marked by a bold black line with ‘significant’ or ‘not significant’ indicated by * or *n.s.* respectively). We used a two-tailed paired *t*-test in bout analyses and spindle analyses, and an unpaired *t*-test to compare control vs KD sIPSCs. All statistics were performed in MATLAB, GraphPad Prism5 or Microsoft Excel.

Data availability

Raw in vivo electrophysiologic data⁶⁰ used in this study are available from the Open Science Framework repository at <https://osf.io/uf2ca/>. Raw in vitro electrophysiologic data⁶¹ used in this study are available from the Open Science Framework repository at <https://osf.io/2k8s3/>. A Source Data file is provided with this paper.

Code availability

Custom code central and original to this manuscript are available from the Open Science Framework repository at <https://osf.io/uf2ca/>.

Received: 26 April 2021; Accepted: 4 April 2022;

Published online: 26 April 2022

References

- Tononi, G. & Cirelli, C. Sleep function and synaptic homeostasis. *Sleep. Med. Rev.* **10**, 49–62 (2006).
- Dworak, M., McCarley, R. W., Kim, T., Kalinchuk, A. V. & Basheer, R. Sleep and brain energy levels: ATP changes during sleep. *J. Neurosci.* **30**, 9007–9016 (2010).
- Xie, L. et al. Sleep drives metabolite clearance from the adult brain. *Science* **342**, 373–377 (2013).
- Dolsen, M. R. et al. Neurophysiological correlates of suicidal ideation in major depressive disorder: hyperarousal during sleep. *J. Affect. Disord.* **212**, 160–166 (2017).
- Stepanski, E., Lamphere, J., Badia, P., Zorick, F. & Roth, T. Sleep fragmentation and daytime sleepiness. *Sleep* **7**, 18–26 (1984).
- Ellis, J. G., Perlis, M. L., Neale, L. F., Espie, C. A. & Bastien, C. H. The natural history of insomnia: focus on prevalence and incidence of acute insomnia. *J. Psychiatr. Res.* **46**, 1278–1285 (2012).
- Luz, G. P. et al. Impaired sustained attention and lapses are present in patients with mild obstructive sleep apnea. *Sleep. Breath.* **20**, 681–687 (2016).
- Sands, S. A. et al. Quantifying the arousal threshold using polysomnography in obstructive. *Sleep. Apnea. Sleep.* **41**, 1–9 (2018).
- Uygun, D. S. et al. Bottom-up versus top-down induction of sleep by zolpidem acting on histaminergic and neocortex neurons. *J. Neurosci.* **36**, 11171–11184 (2016).
- Alexandre, C. et al. Sleep-stabilizing effects of E-6199, compared to zopiclone, zolpidem and THIP in mice. *Sleep* **31**, 259–270 (2008).
- Steriade, M. & McCarley, R. W. *Brainstem control of wakefulness and sleep*, <https://doi.org/10.1007/978-1-4757-4669-3> (New York, Plenum Press, 1990).
- Brown, R. E., Basheer, R., McKenna, J. T., Strecker, R. E. & McCarley, R. W. Control of sleep and wakefulness. *Physiol. Rev.* **92**, 1087–1187 (2012).
- Franks, N. P. General anaesthesia: from molecular targets to neuronal pathways of sleep and arousal. *Nat. Rev. Neurosci.* **9**, 370–386 (2008).
- Steriade, M., Nunez, A. & Amzica, F. Intracellular analysis of relations between the slow (<1 Hz) neocortical oscillation and other sleep rhythms of the electroencephalogram. *J. Neurosci.* **13**, 3266–3283 (1993).
- Jahnsen, H. & Llinás, R. Ionic basis for the electro-responsiveness and oscillatory properties of guinea-pig thalamic neurones in vitro. *J. Physiol.* **349**, 227–247 (1984).
- Jahnsen, H. & Llinás, R. Voltage-dependent burst-to-tonic switching of thalamic cell activity: an in vitro study. *Arch. Ital. Biol.* **122**, 73–82 (1984).
- Lewis, L. D. et al. Thalamic reticular nucleus induces fast and local modulation of arousal state. *Elife* **4**, e08760 (2015).
- Espinosa, F., Torres-Vega, M. A., Marks, G. A. & Joho, R. H. Ablation of Kv3.1 and Kv3.3 potassium channels disrupts thalamocortical oscillations in vitro and in vivo. *J. Neurosci.* **28**, 5570–5581 (2008).
- Joho, R. H., Ho, C. S. & Marks, G. A. Increased gamma- and decreased delta-oscillations in a mouse deficient for a potassium channel expressed in fast-spiking interneurons. *J. Neurophysiol.* **82**, 1855–1864 (1999).
- Thankachan, S. et al. Thalamic reticular nucleus parvalbumin neurons regulate sleep spindles and electrophysiological aspects of schizophrenia in mice. *Sci. Rep.* **9**, 1–16 (2019).
- Herrera, C. G. et al. Hypothalamic feedforward inhibition of thalamocortical network controls arousal and consciousness. *Nat. Neurosci.* **19**, 290–298 (2016).
- Ochoa-Sanchez, R. et al. Promotion of non-rapid eye movement sleep and activation of reticular thalamic neurons by a novel MT 2 melatonin receptor ligand. *J. Neurosci.* <https://doi.org/10.1523/JNEUROSCI.2676-11.2011> (2011).
- Fernandez, L. M. et al. Thalamic reticular control of local sleep in mouse sensory cortex. *Elife* **7**, e39111 (2018).
- Olsen, R. W. & Sieghart, W. GABA A receptors: subtypes provide diversity of function and pharmacology. *Neuropharmacology* **56**, 141–148 (2009).
- Winsky-Sommerer, R. et al. Normal sleep homeostasis and lack of epilepsy phenotype in GABAA receptor $\alpha 3$ subunit-knockout mice. *Neuroscience* <https://doi.org/10.1016/j.neuroscience.2008.03.081> (2008).
- Hörtnagl, H. et al. Patterns of mRNA and protein expression for 12 GABAA receptor subunits in the mouse brain. *Neuroscience* **236**, 345–372 (2013).
- Vega Alanis, B. A. et al. Allosteric GABAA receptor modulators—A review on the most recent heterocyclic chemotypes and their synthetic accessibility. *Molecules* **25**, 999 (2020).
- Huber, R., Deboer, T. & Tobler, I. Effects of sleep deprivation on sleep and sleep EEG in three mouse strains: empirical data and simulations. *Brain Res.* **857**, 8–19 (2000).
- Dossi, R. C., Nuñez, A. & Steriade, M. Electrophysiology of a slow (0.5–4 Hz) intrinsic oscillation of cat thalamocortical neurones in vivo. *J. Physiol.* **447**, 215–234 (1992).
- Nuñez, A., Amzica, F. & Steriade, M. Intrinsic and synaptically generated delta (1–4 Hz) rhythms in dorsal lateral geniculate neurons and their modulation by light-induced fast (30–70 Hz) events. *Neuroscience* **51**, 269–284 (1992).
- Hubbard, J. et al. Rapid fast-delta decay following prolonged wakefulness marks a phase of wake-inertia in NREM sleep. *Nat. Commun.* **2020** **11**, 1–16 (2020).
- Steriade, M., Contreras, D., Dossi, R. C. & Nunez, A. The slow (<1 Hz) oscillation in reticular thalamic and thalamocortical neurons: Scenario of sleep rhythm generation in interacting thalamic and neocortical networks. *J. Neurosci.* **13**, 3284–3299 (1993).
- Uygun, D. S. et al. Validation of an automated sleep spindle detection method for mouse electroencephalography. *Sleep* **42**, 1–13 (2019).
- Kryger, M. H., Roth, T. & Dement, W. C. *Principles and practice of sleep medicine*, <https://doi.org/10.1016/B0-7216-0797-7/X5001-0> (Philadelphia, PA: Elsevier/Saunders, 2005).
- Schwarzer, C. et al. Distribution of the major γ -aminobutyric acid A receptor subunits in the basal ganglia and associated limbic brain areas of the adult rat. *J. Comp. Neurol.* **433**, 526–549 (2001).
- Pirker, S., Schwarzer, C., Wieselthaler, A., Sieghart, W. & Sperk, G. GABAA receptors: Immunocytochemical distribution of 13 subunits in the adult rat brain. *Neuroscience* **101**, 815–850 (2000).
- Gross, A. et al. Differential localization of GABAA receptor subunits in relation to rat striatopallidal and pallidopallidal synapses. *Eur. J. Neurosci.* **33**, 868–878 (2011).
- Wisden, W., Laurie, D. J., Monyer, H. & Seeburg, P. H. The distribution of 13 GABA(A) receptor subunit mRNAs in the rat brain. I. Telencephalon, diencephalon, mesencephalon. *J. Neurosci.* **12**, 1040–1062 (1992).
- Härtig, W., Brauer, K., Fritschy, J. M., Brückner, G. & Bigl, V. Regional and cellular expression sites of the $\alpha 1$ subunit of GABAA receptors in the rat basal forebrain: a cytochemical study with glutamic acid decarboxylase, choline acetyltransferase, calcium-binding proteins and nitric oxide synthase as second markers. *Brain Res.* **692**, 215–226 (1995).
- Platt, R. J. et al. CRISPR-Cas9 knockin mice for genome editing and cancer modeling. *Cell* **159**, 440–455 (2014).
- Hou, G., Smith, A. G. & Zhang, Z.-W. Lack of intrinsic GABAergic connections in the thalamic reticular nucleus of the mouse. *J. Neurosci.* **36**, 7246–7252 (2016).
- Landisman, C. E. et al. Electrical synapses in the thalamic reticular nucleus. *J. Neurosci.* **22**, 1002–1009 (2002).
- Clemente-Perez, A. et al. Distinct thalamic reticular cell types differentially modulate normal and pathological cortical rhythms. *Cell Rep.* <https://doi.org/10.1016/j.celrep.2017.05.044> (2017).
- Huguenard, J. R. & Prince, D. A. Intrathalamic rhythmicity studied in vitro: Nominal T-current modulation causes robust antioscillatory effects. *J. Neurosci.* **14**, 5485–5502 (1994).
- Schofield, C. M., Kleiman-Weiner, M., Rudolph, U. & Huguenard, J. R. A gain in GABAA receptor synaptic strength in thalamus reduces oscillatory activity and absence seizures. *Proc. Natl Acad. Sci. USA.* **106**, 7630–7635 (2009).

46. Landolt, H. P. et al. Zolpidem and sleep deprivation: different effect on EEG power spectra. *J. Sleep. Res.* **9**, 175–183 (2000).
47. Headley, D. B. & Paré, D. Common oscillatory mechanisms across multiple memory systems. *NPJ Sci. Learn.* **2**, 1 (2017).
48. Nutt, D. J. & Stahl, S. M. Searching for perfect sleep: the continuing evolution of GABAA receptor modulators as hypnotics. *J. Psychopharmacol.* **24**, 1601–1612 (2010).
49. Anacleit, C. et al. Effects of GF-015535-00, a novel $\alpha 1$ GABA A receptor ligand, on the sleep-wake cycle in mice, with reference to zolpidem. *Sleep* **35**, 103–111 (2012).
50. Waldvogel, H. J., Munkle, M., van Roon-Mom, W., Mohler, H. & Faull, R. L. M. The immunohistochemical distribution of the GABA A receptor $\alpha 1$, $\alpha 2$, $\alpha 3$, $\beta 2/3$ and $\gamma 2$ subunits in the human thalamus. *J. Chem. Neuroanat.* **82**, 39–55 (2017).
51. Sperk, G. et al. Immunohistochemical distribution of 10 GABAA receptor subunits in the forebrain of the rhesus monkey *Macaca mulatta*. *J. Comp. Neurol.* **528**, 2551–2568 (2020).
52. Swiech, L. et al. In vivo interrogation of gene function in the mammalian brain using CRISPR-Cas9. *Nat. Biotechnol.* **33**, 102–106 (2015).
53. Bae, S., Park, J. & Kim, J.-S. Cas-OFFinder: a fast and versatile algorithm that searches for potential off-target sites of Cas9 RNA-guided endonucleases. *Bioinformatics* **30**, 1473–1475 (2014).
54. Labun, K. et al. CHOPCHOP v3: expanding the CRISPR web toolbox beyond genome editing. *Nucleic Acids Res.* **47**, W171–W174 (2019).
55. Pinault, D. & Deschênes, M. Projection and innervation patterns of individual thalamic reticular axons in the thalamus of the adult rat: a three-dimensional, graphic, and morphometric analysis. *J. Comp. Neurol.* **391**, 180–203 (1998).
56. Franken, P., Malafosse, A. & Tafti, M. Genetic variation in EEG activity during sleep in inbred mice. *Am. J. Physiol.* **275**, 1127–1137 (1998).
57. Prerau, M. J., Brown, R. E., Bianchi, M. T., Ellenbogen, J. M. & Purdon, P. L. Sleep neurophysiological dynamics through the lens of multitaper spectral analysis. *Physiology* **32**, 60–92 (2017).
58. Mochizuki, T. et al. Behavioral state instability in orexin knock-out mice. *J. Neurosci.* **24**, 6291–6300 (2004).
59. Franklin, K. B. J. & Paxinos, G. The mouse brain in stereotaxic coordinates (3rd ed.). (Boston: Elsevier/Academic Press, 2008).
60. Uygun, D. S. et al. In vivo data sets of: knockdown of GABAA alpha3 subunits on thalamic reticular neurons enhances deep sleep in mice. *OSF.* <https://doi.org/10.17605/OSF.IO/UF2CA> (2022).
61. Uygun, D. S. et al. In vitro data sets of: knockdown of GABAA alpha3 subunits on thalamic reticular neurons enhances deep sleep in mice. *OSF.* <https://doi.org/10.17605/OSF.IO/2K8S3> (2022).

Acknowledgements

This work was supported by VA Biomedical Laboratory Research and Development Service Merit Awards I01 BX001404 (R.B.); I01 BX001356 and I01 BX004673 (R.E.B.); I01 BX004500 (J.M.M.); VA CDA IK2 BX004905 (D.S.U.); and NIH support from R01 NS119227 (R.B.) R21 NS079866 (R.B.), R01 MH039683 (R.E.B.), T32 HL07901 (D.S.U.), K01 AG068366 (FK), R21 MH125242 (J.M.M./J.T.M.).

Author contributions

D.S.U.: Conceptualization, Software, Formal analysis, Investigation, Data Curation, Writing – Original Draft, Writing – Review & Editing, Visualization, Supervision,

Funding Acquisition. C.Y.: Conceptualization, Formal analysis, Investigation, Data Curation, Writing – Original Draft, Writing – Review & Editing, Visualization, Funding Acquisition. E.R.T.: Conceptualization, Formal analysis, Investigation, Data Curation, Writing – Review & Editing. F.K.: Conceptualization, Software, Formal analysis, Investigation, Writing – Review & Editing, Supervision. E.L.H.: Investigation, Data Curation, Writing – Editing. E.R.T.: Conceptualization, Investigation, Data Curation. J.T.M.: Formal analysis, Investigation, Visualization, Writing – Review & Editing. J.M.M.: Conceptualization, Software, Writing – Review & Editing, Supervision, Funding Acquisition. R.E.B.: Conceptualization, Resources, Data Curation, Writing – Original Draft, Writing – Review & Editing, Visualization, Supervision, Project administration, Funding Acquisition. R.B.: Conceptualization, Resources, Data Curation, Writing – Original Draft, Writing – Review & Editing, Visualization, Supervision, Project administration, Funding Acquisition.

Competing interests

D.S.U., J.T.M., J.M.M., R.E.S. and R.B. are Research Health Scientists at VA Boston Healthcare System, West Roxbury, MA. The contents of this work do not represent the views of the US Department of Veterans Affairs or the United States Government. J.T.M. received partial salary compensation and funding from Merck MISP (Merck Investigator Sponsored Programs) but has no conflict of interest with this work. Other authors declare no competing interests.

Additional information

Supplementary information The online version contains supplementary material available at <https://doi.org/10.1038/s41467-022-29852-x>.

Correspondence and requests for materials should be addressed to Radhika Basheer.

Peer review information *Nature Communications* thanks Yunlei Yang, Jelena Radulovic and the other anonymous reviewer(s) for their contribution to the peer review of this work.

Reprints and permission information is available at <http://www.nature.com/reprints>

Publisher's note Springer Nature remains neutral with regard to jurisdictional claims in published maps and institutional affiliations.



Open Access This article is licensed under a Creative Commons Attribution 4.0 International License, which permits use, sharing, adaptation, distribution and reproduction in any medium or format, as long as you give appropriate credit to the original author(s) and the source, provide a link to the Creative Commons license, and indicate if changes were made. The images or other third party material in this article are included in the article's Creative Commons license, unless indicated otherwise in a credit line to the material. If material is not included in the article's Creative Commons license and your intended use is not permitted by statutory regulation or exceeds the permitted use, you will need to obtain permission directly from the copyright holder. To view a copy of this license, visit <http://creativecommons.org/licenses/by/4.0/>.

This is a U.S. government work and not under copyright protection in the U.S.; foreign copyright protection may apply 2022